

# A Process Model of Rho GTP-binding Proteins

Luca Cardelli <sup>1</sup>

*Microsoft Research  
7 JJ Thomson Avenue, CB3 0FB, Cambridge, UK*

Emmanuelle Caron

*Centre for Molecular Microbiology and Infection  
Imperial College, London, UK*

Philippa Gardner

*Department of Computing  
Imperial College, London, UK*

Ozan Kahramanoğulları <sup>2</sup>

*Department of Computing &  
Centre for Integrative Systems Biology  
Imperial College, London, UK*

Andrew Phillips

*Microsoft Research  
7 JJ Thomson Avenue, CB3 0FB, Cambridge, UK*

---

## Abstract

Rho GTP-binding proteins play a key role as molecular switches in many cellular activities. In response to extracellular stimuli and with the help from regulators (GEF, GAP, Effector, GDI), these proteins serve as switches that interact with their environment in a complex manner. Based on the structure of a published ordinary differential equations (ODE) model, we first present a generic process model for the Rho GTP-binding proteins, and compare it with the ODE model. We then extend the basic model to include the behaviour of the GDIs and explore the parameter space for the extended model with respect to biological data from the literature. We discuss the challenges this extension brings and the directions of further research. In particular, we present techniques for modular representation and refinement of process models, where, for example, different Rho proteins with different rates for regulator interactions can be given as the instances of the same parametric model.

*Keywords:* GTP-binding proteins, stochastic  $\pi$ -calculus, process modeling

---

# 1 Introduction

The Rho GTP-binding proteins constitute a distinct family within the super-family of Ras-related small GTPases with twenty-two identified mammalian members, including Rho, Rac and Cdc42 [16]. These proteins serve as molecular switches in various subcellular activities, regulating a variety of cell functions, including actin dependent processes such as cell adhesion, cell motility, cell shape changes and phagocytosis [1]. When activated by the binding of GTP, these proteins transmit an incoming signal further to downstream effectors.

Rho GTP-binding proteins play an important role in phagocytosis because of their role in regulating actin [5] dependent protrusion of the membrane around the internalised particles. Phagocytosis is a form of endocytosis by which a cell engulfs micro-organisms, large edible particles and cellular debris. Phagocytosis literally means ‘cell eating’. Single-celled organisms such as amoeba obtain food in this way. Phagocytosis occurs in multi-cellular organisms where, for example, macrophages and other white blood cells (professional phagocytes) defend the body against invasions of harmful viruses, bacteria, cancerous body cells, and other threats to health [1]. Phagocytosis and its sub-processes play a key role in host-pathogen interactions. The mechanisms involved in the recognition and uptake of these pathogens by professional phagocytes is crucial for the induction of protective immunity.

Our long term goal, along these lines, is providing a systems-level understanding of these cellular processes by incrementally building more refined models reflecting their mechanistic behaviour. In this paper, we use the stochastic  $\pi$ -calculus (see, e.g., [24]) to provide a compositional and scalable notation for modelling the Rho GTP-binding proteins at the core of phagocytosis.

We study Goryachev and Pokhilko’s paper [13] on an ordinary differential equation (ODE) analysis of the Rho GTP-binding protein cycle, first in isolation and then with their regulators GEF and GAP. For this purpose, we introduce an extension of the stochastic  $\pi$ -calculus which provides a more modular means for extending and refining the models. With this extension to the calculus, our process model provides a simple modular description of the Rho GTP-binding protein cycle, where the structure of the model naturally follows the structure of the biological model. Using the Stochastic Pi Machine (SPiM) [21,20] and the rates of interaction described in [13], we provide simulations which precisely mimic the results given using ODEs. Following [13], we also extend our model to include the effectors which interact with these proteins at the membrane. Again, our results remain consistent with the results obtained from the ODE analysis. This result provides an essential starting point for our investigation of the behaviour of the Rho GTP-binding proteins using process models.

We further extend our model to include the interactions of the GTP-binding

---

<sup>1</sup> The authors would like to thank Vassily Lyutsarev from Microsoft Research, for implementing and managing the parameter exploration process on a cluster of machines and the anonymous referees for helpful comments and suggestions. Cardelli acknowledges support of a visiting professorship at Imperial College. Gardner acknowledges support of a Microsoft Research Cambridge/Royal Academy of Engineering Senior Fellowship. Kahramanoğlu acknowledges support of the UK Biotechnology and Biological Sciences Research Council through the Centre for Integrative Systems Biology at Imperial College (grant BB/C519670/1).

<sup>2</sup> To whom correspondence should be addressed. Email: ozank@doc.ic.ac.uk

proteins with another class of regulators called GDIs, which were not included in the ODE analysis of [13]. Our initial aim was to analyse the two biological models described in the survey paper [8], but instead we introduce a hybrid model which fits more closely with the current knowledge on these proteins. Based on the recent biological literature, we use our model to compare and analyse the different views of the interactions of the GDIs with the Rho family proteins. In order to compare these different views, we study the effect of varying the parameters of the extended model with different initial quantities of the species of the model. We then provide a systematic study of the rates of the extended model by using SPiM to explore the parameter space, and explain the simulation behaviour with respect to data from the literature.

Because our model reflects the mechanistic behaviour of the Rho GTP binding proteins, it can be used to model different members of the Rho family proteins acting in the same biological process. As another contribution of this paper, we introduce a technique on process models which allows to use them modularly, for example, to include different members of the Rho family proteins with different interaction rates in the same simulation as instances of the same parametrised model. Thus, this technique makes it possible to easily include a model with a certain structure with different instances of rates in the same simulation. Because cellular events such as Fc receptor-mediated phagocytosis involves different members of the Rho family proteins, this technique is useful in modelling such larger biological systems such as signalling cascades where different members of Rho family proteins act in concert.

Our process model of Rho GTP binding proteins provides a formal executable representation of these proteins together with their regulators. Due to its compositionality, our model should thus stimulate a research environment where models are modified and extended easily at will to perform biological experiments *in silico* in order to guide the wet-lab experiments. In such a setting, wet-lab experiments then corroborate and provide data for more accurate process models by adding more detail to certain components or by extending the biological system being considered.

## 2 Rho GTP-binding Proteins and their Role in Fc Receptor-mediated Phagocytosis

Phagocytosis is the process whereby cells engulf large particles, usually over  $0.5\mu m$  in diameter, by a mechanism that is based on the local rearrangement of the actin cytoskeleton. Phagocytosis plays an essential role in host defence against invading pathogens, and in clearance of cell corpses generated by programmed cell death or apoptosis. Phagocytosis contributes to inflammation and the immune response [1].

Phagocytosis is a triggered process, often initiated by the interaction of particle-bound ligands (opsonins) with specific receptors on the cell membrane of ‘professional’ phagocytic white blood cells such as macrophages, neutrophils and dendritic cells [6]. Among the variety of surface proteins dedicated to phagocytosis, Fc receptors (FcRs) and receptors for complement fragments (Cr’s) mediate the clearance of pathogens covered by the specific antibody or complement respectively [15].

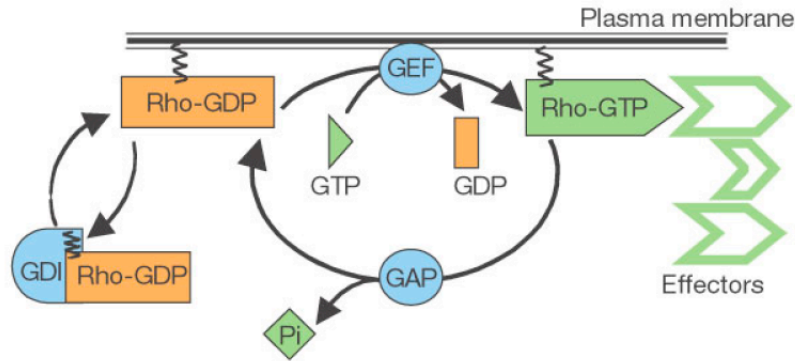


Fig. 1. Rho GTP-binding protein cycle. Reproduced with permission from Macmillan Publishers Ltd: *Nature* [10], copyright 2002.

### 2.1 *Fc Receptor-mediated Phagocytosis*

In the context of Fc receptor-mediated phagocytosis, the signalling cascade is triggered by antibodies, called immunoglobulin, for example, IgG, which protect the organism by binding to the surface of infectious micro-organisms to form a coat. In this situation, the tail region of each antibody molecule, called the *Fc region*, is exposed on the exterior. This antibody coat is recognised by specific *Fc receptors* on the surface of the cell. Their binding induces the phagocytic cell to extend pseudopods and extend its tips to form a phagosome while proceeding with binding its ligands in a zipper-like fashion around the internalised particle [11].

As a result of FcR-Fc interaction on the exterior surface of the cell membrane, a protein tyrosine kinase of the Src family is activated. Following this, Src phosphorylates two tyrosine residues on the receptor's signalling subunits located on the internal tail of the Fc receptor. These tyrosine residues belong to immunoreceptor tyrosine-based activation motifs, or ITAMs. Another protein tyrosine kinase, Syk, is then recruited through its Src-homology 2 (SH2) domains by binding to the phosphorylated ITAMs. This results in autophosphorylation and activation of Syk. Among other tasks, activated Syk is responsible for the recruitment of the protein Vav [15], which then activates the Rho GTP-binding protein Rac. In a parallel independent pathway, another Rho GTP-binding protein Cdc42 gets activated by an unknown protein [19]. Cdc42 and Rac then act at distinct stages to promote actin filament polymerisation and organisation at the site of particle ingestion: Cdc42 and Rac control actin filament polymerisation through proteins WASP (Wiskott-Aldrich Syndrome protein) and WAVE, respectively, that bind to and stimulate the activity of the Arp2/3 complex. Activation of Arp2/3 results in actin polymerisation and the extrusion of actin based protrusion around the internalised particle formed. While Rac is generally responsible for the branching structure of actin filaments, Cdc42 causes the actin to polymerise in a linear structure [27].

### 2.2 *Rho GTP-binding Proteins in Fc Receptor-mediated Phagocytosis*

The proteins Cdc42 and Rac mentioned above belong to the Rho GTP-binding proteins. As in the context of phagocytosis, the family of Rho GTP-binding proteins serve as molecular switches in various subcellular activities, regulating a variety of

cell functions, including actin organisation and cell shape, cell adhesion, cell motility, membrane trafficking and gene expression [6,3]. These proteins can be perceived as regulating the transmission of an incoming signal further to some effector in a molecular module by cycling between inactive and active states, depending on being GDP or GTP bound, respectively. As depicted in Figure 1, GDP/GTP cycling is regulated by guanine nucleotide exchange factors (GEFs) that promote the GDP dissociation and GTP-binding, whereas GTPase-activating proteins (GAPs) have the opposite effect and stimulate the hydrolysis of Rho GTP into Rho GDP. In the active GTP-bound state, Rho proteins interact with and activate downstream effectors, for example, to control actin polymerisation in the context of Fc receptor mediated phagocytosis [16]. Although the role of GDIs (Guanine Nucleotide dissociation Inhibitors) during phagocytosis or cell processes in general is not totally clear, there is evidence that these proteins are responsible for multiple tasks in the regulation of Rho GTP-binding proteins, including the inhibition of the GTP hydrolysis into GDP (see Section 4).

### 2.3 An ODE Model of Rho GTP-binding Proteins

In [13], Goryachev and Pokhilko give a computational model of the Rho GTP-binding proteins by means of ordinary differential equations (ODE). The structure of their model is given in Figure 2. In Figure 2, R denotes the Rho GTP-binding protein, whereas RD and RT denote its GDP and GTP bound forms respectively. A and E denote GAP and GEF, respectively. Thus, RDE, for example, denotes the protein complex formed by RD and E. The ODEs for this model given in [13] are as follows.<sup>3</sup>

$$\begin{aligned}
[\text{RD}]^\bullet &= k_{81} \cdot \text{RDA} - k_{18} \cdot \text{RD.A} + k_{31} \cdot \text{RDE} - k_{13} \cdot \text{RD.E} + k_{91} \cdot \text{R.D} - k_{19} \cdot \text{RD} + k_{21} \cdot \text{RT} \\
[\text{RT}]^\bullet &= k_{52} \cdot \text{RTE} - k_{25} \cdot \text{RT.E} + k_{92} \cdot \text{R.T} - k_{29} \cdot \text{RT} - k_{21} \cdot \text{RT} + k_{62} \cdot \text{RTA} - k_{26} \cdot \text{RT.A} \\
[\text{RDE}]^\bullet &= k_{13} \cdot \text{RD.E} - k_{31} \cdot \text{RDE} + k_{43} \cdot \text{RE.D} - k_{34} \cdot \text{RDE} + k_{53} \cdot \text{RTE} \\
[\text{RE}]^\bullet &= k_{34} \cdot \text{RDE} - k_{43} \cdot \text{RE.D} + k_{54} \cdot \text{RTE} - k_{45} \cdot \text{RE.T} + k_{94} \cdot \text{R.E} - k_{49} \cdot \text{RE} \\
[\text{RTE}]^\bullet &= k_{45} \cdot \text{RE.T} - k_{54} \cdot \text{RTE} + k_{25} \cdot \text{RT.E} - k_{52} \cdot \text{RTE} - k_{53} \cdot \text{RTE} \\
[\text{RTA}]^\bullet &= k_{26} \cdot \text{RT.A} - k_{62} \cdot \text{RTA} - k_{68} \cdot \text{RTA} + k_{76} \cdot \text{RA.T} - k_{67} \cdot \text{RTA} \\
[\text{RA}]^\bullet &= k_{67} \cdot \text{RTA} - k_{76} \cdot \text{RA.T} + k_{97} \cdot \text{R.A} - k_{79} \cdot \text{RA} + k_{87} \cdot \text{RDA} - k_{78} \cdot \text{RA.D} \\
[\text{RDA}]^\bullet &= k_{68} \cdot \text{RTA} + k_{78} \cdot \text{RA.D} - k_{87} \cdot \text{RDA} + k_{18} \cdot \text{RD.A} - k_{81} \cdot \text{RDA} \\
[\text{R}]^\bullet &= k_{29} \cdot \text{RT} - k_{92} \cdot \text{R.T} + k_{49} \cdot \text{RE} - k_{94} \cdot \text{R.E} + k_{19} \cdot \text{RD} - k_{91} \cdot \text{R.D} + k_{79} \cdot \text{RA} - k_{97} \cdot \text{R.A} \\
[\text{E}]^\bullet &= k_{31} \cdot \text{RDE} - k_{13} \cdot \text{RD.E} + k_{52} \cdot \text{RTE} - k_{25} \cdot \text{RT.E} + k_{49} \cdot \text{RE} - k_{94} \cdot \text{R.E} \\
[\text{A}]^\bullet &= k_{81} \cdot \text{RDA} - k_{18} \cdot \text{RD.A} + k_{62} \cdot \text{RTA} - k_{26} \cdot \text{RT.A} + k_{79} \cdot \text{RA} - k_{97} \cdot \text{R.A}
\end{aligned}$$

In this model, the authors study GTP-binding proteins in isolation, disregarding the GDIs. The ODE model uses mainly the quantitative biochemical data on Cdc42p. This results in an explanation of the experimentally observed rapid cycling of Rho GTP-binding proteins while having high activity. In this paper, based on this ODE model, we give a process calculus model which compositionally builds and extends the ODE model, and provide a comparison of the two models.

<sup>3</sup> The ODE for  $[\text{RDE}]^\bullet$  is slightly modified to correct a minor typo with respect to the one given in [13].

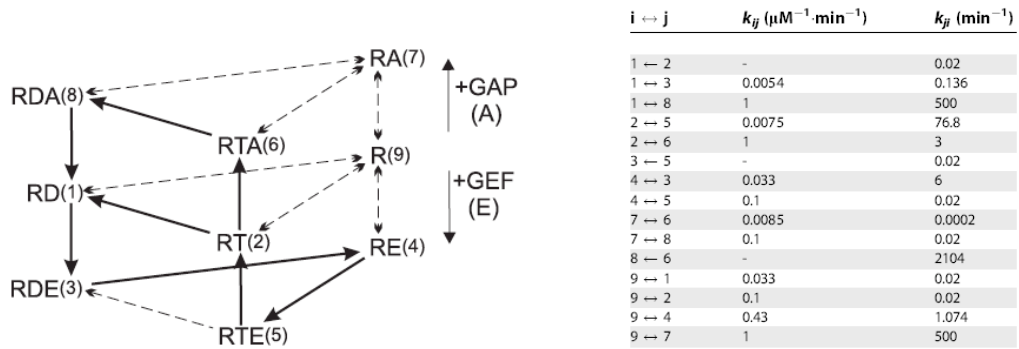


Fig. 2. The ODE model given in [13]. The diagram on the left depicts the chemical reactions underlying the ODEs for this model. The rates that are used in [13] with respect to data collected from the literature are given on the right.

### 3 A Process Calculus Model

We compositionally build a process model of Rho GTP-binding proteins by treating the components of the Rho GTP cycle as components of a stochastic  $\pi$ -calculus process (see, e.g., [24,2]). For this purpose, we introduce an extension of the stochastic  $\pi$ -calculus which provides a more modular means for the construction of the models by allowing the association of stochastic weights to actions. By resorting to this new capability, we first build a basic model, and then modularly extend it with regulators. At each stage, we provide simulations of our models and compare our results with the corresponding ODE model [13].

#### 3.1 Biological Processes as Computations

In the stochastic  $\pi$ -calculus, the basic building blocks are processes. Each process has a precise description of what actions it can take. Once a biological system has been modelled using these basic components, we can run a stochastic simulation on the model in order to display an evolution of the considered system over time. In this paper, the simulations are performed using the Stochastic Pi Machine (SPiM) <sup>4</sup> [21], which serves as a platform for implementing stochastic  $\pi$ -calculus processes and for running machine simulations.

When modelling biological processes in the stochastic  $\pi$ -calculus, as introduced in [25], it is sufficient to associate each channel name a fixed rate. In such a setting, each channel corresponds to a separate interaction between two entities, and does not explicitly allow multiple interactions on the same channel to occur at different rates. However, such an assumption limits the modularity of the modelling approach, since it requires a new channel to be created for each variation in the interaction rate. In this subsection, by adding a layer of abstraction that decouples the interaction rate from the ability to interact, we extend the calculus such that actions are associated with stochastic weights. Thus, the extended calculus helps to regulate the creation of channels while building models and, thereby, improves modularity.

The syntax of the stochastic  $\pi$ -calculus (SPi) with weights is shown in Defini-

<sup>4</sup> <http://research.microsoft.com/~aphillip/spim/>

tion 3.1. It is similar to the SPi syntax presented in [21]. The reduction rules of the calculus are given in Definition 3.2. Each rule is labelled with a corresponding rate that denotes the rate of a single reaction, which can be either a communication or a delay. The rules are standard except for the communication rule 2, where the rate of the communication is given by the rate of the channel multiplied by the weights of the input and output actions.

We use a version of the SPiM, which implements the SPi calculus with weights, given in Definition 3.1, Definition 3.2 and Definition 3.3: a process  $P$  can choose, stochastically, between zero or more alternative behaviours. In the language of SPiM, choice of  $N$  processes is written as  $\text{do } P_1 \text{ or } \dots \text{ or } P_N$ . A choice of only one process is written as  $P_1$ , while the empty choice is written as  $()$ . A parallel composition of  $N$  processes is written as  $P_1 \mid \dots \mid P_N$ . This constitutes the basic form of compositionality, which allows processes to be composed incrementally in order to construct larger system models. A process  $P$  can also be given a name  $X$  with parameter  $m$ , written  $\text{let } X(m) = P$ .

A process can perform a delay at rate  $r$  and then do  $P$ , written  $\text{delay}@r;P$ . The rate  $r$  is a real number value denoting the rate of an exponential distribution, such that the average duration of the delay is  $1/r$ . A process can also send a value  $n$  on channel  $x$  with weight  $r_1$  and then do  $P_1$ , written  $!x(n)*r_1;P_1$ , or it can receive a value  $m$  on channel  $x$  with weight  $r_2$  and then do  $P_2$ , written  $?x(m)*r_2;P_2$ . With respect to the reduction semantics of SPi given in Definition 3.2, if these complementary send and receive actions are running in parallel, they can synchronise on the common channel  $x$  and evolve to  $P_1 \mid P_2\{m:=n\}$ , where  $m$  is replaced by  $n$  in process  $P_2$ . This allows messages to be exchanged from one process to another. The weights  $r_1, r_2$  give a measure of the average time it takes to complete the output and input actions, respectively. In addition, each channel name  $x$  is associated with an underlying rate given by  $\rho(x)$ . The resulting rate of the interaction is given by  $\rho(x)$  times the weights  $r_1$  and  $r_2$ . These weights decouple the ability of two processes to interact on a given channel  $x$  from the rate of the interaction, which can change over time depending on the evolution of the processes. If no weight is given then a default weight of 1 is used. The operator  $\text{new } x@r:t$   $P$  creates a fresh channel  $x$  of rate  $r$  to be used in the process  $P$ , where  $t$  is the type of the channel. For example, the type  $\text{chan}(\text{chan}, \text{chan})$  denotes a channel that can transmit the names of two channels. When a process is prefixed with the declaration of a fresh channel, that channel remains private to the process and does not conflict with any other channel.

In the case where a weight  $r$  is an integer, the process  $?x(m)*r;Q$  can be viewed as a syntactic abbreviation for a choice of  $r$  processes  $\text{do } ?x(m);Q \text{ or } \dots \text{ or } ?x(m);Q$ , which is  $r$  times more likely to occur as the single process  $?x(m);Q$ . And similarly for the output process. This follows from the sum rule of stochastic pi-calculus, based on the fact that exponential distributions are closed under min: the min of two exponential distributions is an exponential distribution whose rate is the sum of the rates. Further, we can generalise integer weights to real-number weights, so that for example  $?x(m)*2.5;Q$  represents a transition at 2.5 times the rate of the single process  $?x(m);Q$ .

In Subsection 3.3, we give a comparison of the stochastic  $\pi$ -calculus with this

---

$P, Q ::=$	$M$	Choice	$E ::=$	$\emptyset$	Empty
	$  X(\tilde{n})$	Instance		$  E, X(\tilde{m}) = P$	Definition
	$  P   Q$	Parallel			$\text{fn}(P) \subseteq \tilde{m}$
	$  \nu x P$	Restriction			
$M ::=$	$\mathbf{0}$	Null	$\pi ::=$	$?x(\tilde{m})_r$	Input
	$  \pi.P + M$	Action		$!x(\tilde{n})_r$	Output
				$  \tau_r$	Delay

---

**Definition 3.1** Syntax of SPi with weights. *Each channel name  $x$  is associated with a rate  $\rho(x)$ .*

---

$$\tau_r.P + M \xrightarrow{r} P \quad (1)$$

$$!x(\tilde{n})_r.P + M \mid ?x(\tilde{m})_s.Q + N \xrightarrow{\rho(x) \cdot r \cdot s} P \mid Q_{\{\tilde{n}/\tilde{m}\}} \quad (2)$$

$$P \xrightarrow{r} P' \Rightarrow \nu x P \xrightarrow{r} \nu x P' \quad (3)$$

$$P \xrightarrow{r} P' \Rightarrow P \mid Q \xrightarrow{r} P' \mid Q \quad (4)$$

$$Q \equiv P \xrightarrow{r} P' \equiv Q' \Rightarrow Q \xrightarrow{r} Q' \quad (5)$$

**Definition 3.2** Reduction in SPi with weights.

---

$$P \mid \mathbf{0} \equiv P \quad (6) \qquad \nu x \mathbf{0} \equiv \mathbf{0} \quad (10)$$

$$P \mid Q \equiv Q \mid P \quad (7) \qquad \nu x \nu y P \equiv \nu y \nu x P \quad (11)$$

$$P \mid (Q \mid R) \equiv (P \mid Q) \mid R \quad (8) \qquad \nu x (P \mid Q) \equiv P \mid \nu x Q \text{ if } x \notin \text{fn}(P) \quad (12)$$

$$X(\tilde{n}) \equiv P_{\{\tilde{n}/\tilde{m}\}} \text{ if } X(\tilde{m}) = P \quad (9)$$

**Definition 3.3** Structural Congruence Axioms in SPi with weights. *Structural congruence is defined as the least congruence that satisfies these axioms. Processes in SPi are assumed to be equal up to renaming of bound names and reordering of terms in a choice.*

---

extended calculus from the point of view modularity. However, as an example for the modelling of chemical reactions using processes [24], consider the situation where the biological species RD and E can interact to form a RDE complex, which can then split to form RD and E. We depict this as the reaction  $\text{RD} + \text{E} \xrightleftharpoons{r'} \text{RDE}$ . This reaction can be read in Figure 2 as the arrow from RD to RDE together with the arrow for E (GEF). Following the results in [13], we know that the binding reaction has rate <sup>5</sup>  $r = 0.0054 \mu\text{M}^{-1} \text{min}^{-1}$ , whereas the unbinding has rate  $r' = 0.136 \text{min}^{-1}$ . This system is coded in SPiM as follows, with processes RD, RDE, E, and ERD. The textual representation on the left is equivalent to the graphical representation on the right, using the graphical representation of the SPiM language presented in [20]:

<sup>5</sup>  $M$  is the unit of measurement for concentration, that is, the number of Moles (the Avogadro's number –  $6.02 * 10^{23}$ ) of solute per litre of solution.

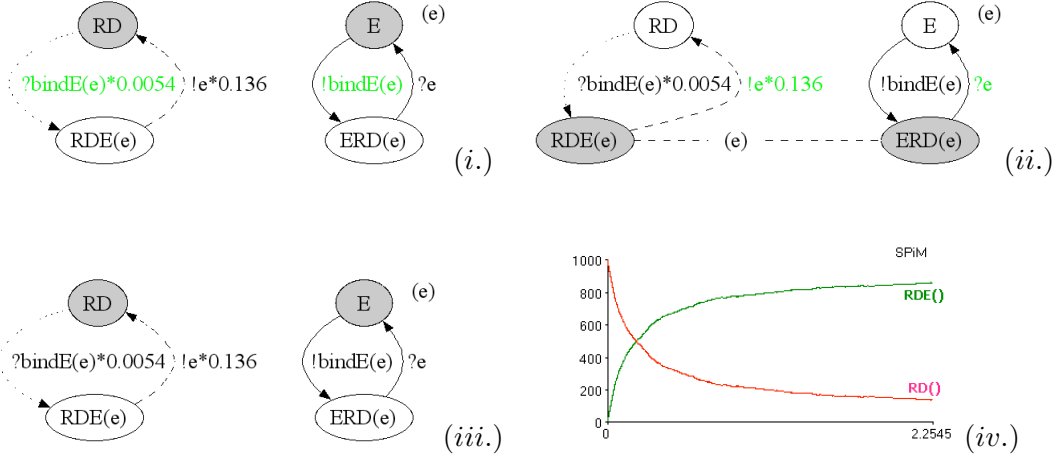
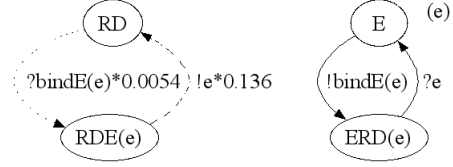


Fig. 3. Graphical representation of the evolution of the RD and E interaction model. Processes RD and E coexist and they can interact on channel  $bindE$  (i.). When they interact, E sends the private channel  $e$ , and RD receives it. This way, they evolve to processes ERD( $e$ ) and RDE( $e$ ), respectively, which share the private channel  $e$ , representing a bond between two bio-chemical species (ii.). By interacting on channel  $e$ , they evolve back to the processes E and RD, respectively (iii.). The SPiM plots of a simulation of the process are shown in (iv.). The  $x$ -axis is the time in minutes and  $y$ -axis is the number of processes. The simulation is started with 1000 RD and 1000 E.

```

let RD() =
  ?bindE(e)*0.0054; RDE(e)
and RDE(e:chan) = !e*0.136; RD()
let E() = (
  new e@1.0: chan()
  !bindE(e); ERD(e) )
and ERD(e:chan) = ?e; E()

```



The first and second lines of the code state that the process RD can receive a channel  $e$  on channel  $bindE$  at rate 0.0054, and then evolve to process RDE( $e$ ), which can send a message on channel  $e$  at rate 0.136 and then evolve to RD. The remaining lines state that process E can send the private channel  $e$  on channel  $bindE$  and then evolve to ERD( $e$ ), which can receive a message on channel  $e$  and then evolve to E. In contrast to the chemical reaction model, instead of using a single process to represent the RDE complex, the calculus uses two separate processes to represent the bound forms of RDE( $e$ ) and ERD( $e$ ), which synchronise on a shared channel  $e$  in order to unbind.

In the graphical representation, following [20], the thickness of the lines is used to indicate the strength of the weights. A normal thickness indicates a default weight of 1.0, while a dashed line indicates a weight between 0.1 and 1.0, and a dotted line indicates a weight less than 0.1.

Throughout the simulations presented in this paper, we have converted the mass action rates, given in [13], to the stochastic rates in the usual way to be used in the Gillespie algorithm [12] implemented in SPiM. We have applied a scaling factor to the number of molecules and to the binary reaction rates. This scaling factor is determined by the number of molecules that are sufficient for a meaningful and inexpensive stochastic simulation (see Subsection 3.3).

Figure 3 shows a run of a cycle of this reaction in the style of the graphical rep-

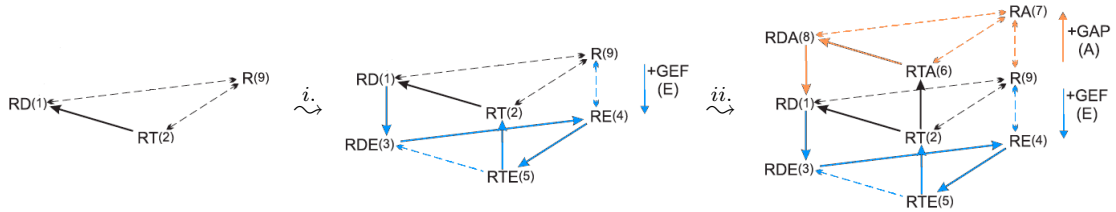


Fig. 4. A graphical representation of modular construction of the interactions of Rho GTP-binding proteins with respect to the ODE model in [13]. A basic model excluding the regulators GEF (E) and GAP (A) is extended first with GEF (*i.*) and then with GAP (*ii.*).

resentation of the SPiM language. The system is represented as two processes that interact over shared channels, where grey nodes indicate actively running processes, and green (lighter) labels indicate the active channel on which the next reaction will be performed. When we run a simulation of this system with initial amounts of 1000 RD and 1000 E ( $RD_0 = 1000$  and  $E_0 = 1000$ ), we get the plot in Figure 3(*iv.*), where red and green are used for RD and RDE molecules, respectively. We can read from this plot the *recovery time*, that is, the time necessary for the system to reach a steady state, as approximately 2.1 mins. At steady state, the *activity* of RDE is given by the ratio of bound RDE over the initial population  $RD_0$ , and is equal to 0.86. These two notions of recovery time and activity will be used in the remainder of the paper.

### 3.2 Rho GTP-binding Proteins without GEF and GAP

As a first step towards building a model of Rho GTP-binding proteins, we consider these proteins in isolation, disregarding the regulators GEF and GAP. This corresponds to the left-most graph in Figure 4.

In this graph, the reactions from R to RD and from R to RT are reversible, but the reaction from RT to RD is in one direction only, since GTP molecules can hydrolyse to GDP molecules by the disassociation of a phosphate group, but re-association of the phosphate group to GDP is not possible. Similar to the model in [13], we do not include the interactions with the GTP and GDP molecules explicitly. Instead, we multiply the reaction rate from R to RD by the number of GDP molecules (D), and similarly the reaction rate from R to RT by the number of GTP molecules (T). This is acceptable because the number GDP and GTP molecules remains relatively constant over time, with concentrations of  $500\mu M$  for GTP and  $50\mu M$  for GDP, as reported in the literature. The SPiM code for this model is given in the left column of Figure 7, where  $D=50.0$  and  $T=500.0$ . The graphical representation at the top is equivalent to the textual representation at the bottom. The process R can evolve to RD or RT with the rates  $0.033*D$  and  $0.1*T$ , respectively. RD can evolve to R with rate 0.02, and RT can evolve to R or RD with rate 0.02 in both cases. As with the example in Subsection 3.1, the thickness of the lines is used to indicate the rates of the different reactions.

When we run a simulation using this code with 1000 R ( $R_0 = 1000$ ), we obtain the left-most plot in Figure 5. We can then read from this plot that the recovery time,

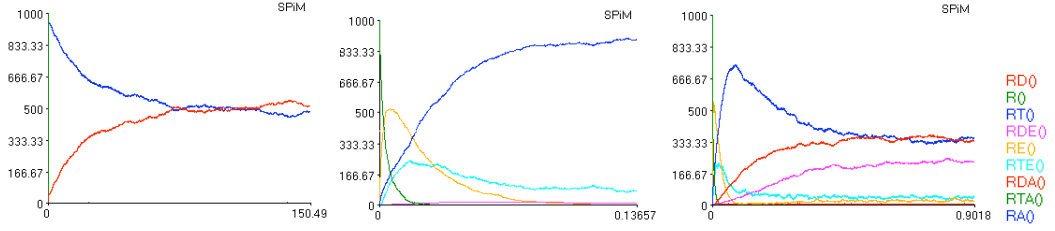


Fig. 5. SPiM plots of simulations for Figure 7 and 15. The  $x$ -axis is the time in minutes and  $y$ -axis is the number of processes. The legend on the right is for all the three plots, where red, green, blue, pink, yellow, and light blue colours are used for RD, R, RT, RDE, RE, and RTE molecules, respectively.

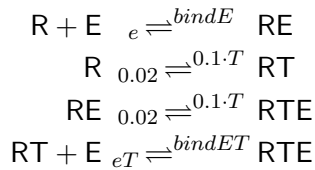
that is, the time necessary for the system to reach stable state, is approximately 90 mins. At the stable state, the RT/R<sub>0</sub> ratio is 0.5.

### 3.3 Rho GTP-binding Proteins with GEF and without GAP

The stochastic  $\pi$ -calculus, as in [25,21], allows a biological model to be constructed in a modular fashion, starting with a simplified description of individual components and progressively refining this description with increasing levels of detail. For example, to construct a process model of Rho GTP (R) binding with GEF (E), we can start with a simplified model of binding and unbinding of R and E:



This is modelled in stochastic  $\pi$ -calculus by defining a separate process for R and E as shown in Figure 6(i), where channels  $bindE$  and  $e$  have the same rates as  $bindE$  and  $e$  in (13). The stochastic  $\pi$ -calculus model allows the behaviour of Rho GTP to be modified independently of the behaviour of GEF, for example by introducing new interactions between Rho GTP and other proteins, without modifying the behaviour of GEF. However, the modularity of the approach is limited by the fact that any change in the GEF binding or unbinding rates in the model for Rho GTP will require a corresponding change in the model for GEF. For example, let us extend the model given with (13) such that there are reactions from R to RT and from RE to RTE, with different binding and unbinding rates with respect to those of (13).



In the corresponding stochastic  $\pi$ -calculus model of Figure 6(ii), we need to communicate two channels ( $e$  and  $e_T$ ) instead of one to model the different unbinding rates of Rho GTP from GEF. In addition, we need to define two channels ( $bindE$  and  $bindET$ ) instead of one channel in order to model the different binding rates.

In this view of the stochastic  $\pi$ -calculus, any change in the interaction rates between Rho GTP and GEF will require a change in the behaviour of both models, which limits the modularity of the approach. The modularity of processes can be improved by decoupling the existence of an interaction from its rate. In the following, we use the stochastic  $\pi$ -calculus with weights, introduced in Subsection 3.1, to exploit this idea in order to gradually extend the models presented.

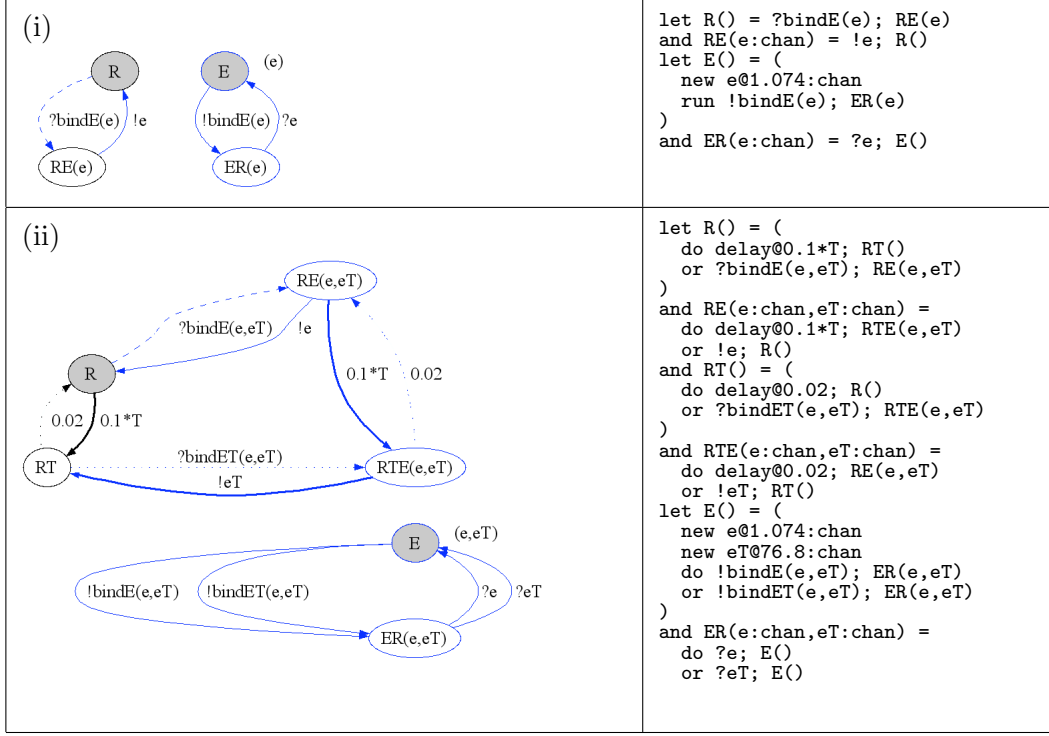


Fig. 6. An example for the progressive refinement of a stochastic  $\pi$ -calculus model of Rho GTP binding with GEF. For each of the models, the graphical representation on the left is equivalent to the textual representation on the right.

We extend the Rho GTP-binding protein process model, given in Subsection 3.2, to a process that also models GEF regulation. This corresponds to the middle diagram in Figure 4 and to the process model given in the last two columns of Figure 7. Here we have two interacting processes, one for the Rho GTP-binding protein and one for GEF (E). The graphical representation at the top is equivalent to the textual representation at the bottom.

As illustrated in this model, the use of weights allows us to write significantly more compact models. In particular, we can define a molecule E that sends on a single channel `bindE`, and a molecule R that receives on this channel at different rates, depending on whether it is bound to D or T. In the general case this reduces the number of channels required in the system, since only a single channel is needed per interaction, regardless of the rate, instead of requiring a separate channel for each interaction at a specific rate. This also reflects the biological intuition of the model, since the ability of two molecules to interact is often characterised by a single binding site, while the strength of the interaction depends on other factors such as changes in the conformation of this site.

When we run a simulation using this code with 1000 R and 1000 E processes ( $R_0 = 1000$  and  $E_0 = 1000$ ), we get the middle plot in Figure 5. We can then read from this plot that the recovery time, that is, the time necessary for the system to reach stable state, is approximately 0.12 mins. At the stable state, the  $RT/R_0$  ratio is 0.87.

In order to compare our process model with the ODE model given in [13], we ran the SPiM simulations on a range of initial number of molecules, where  $R_0$  and

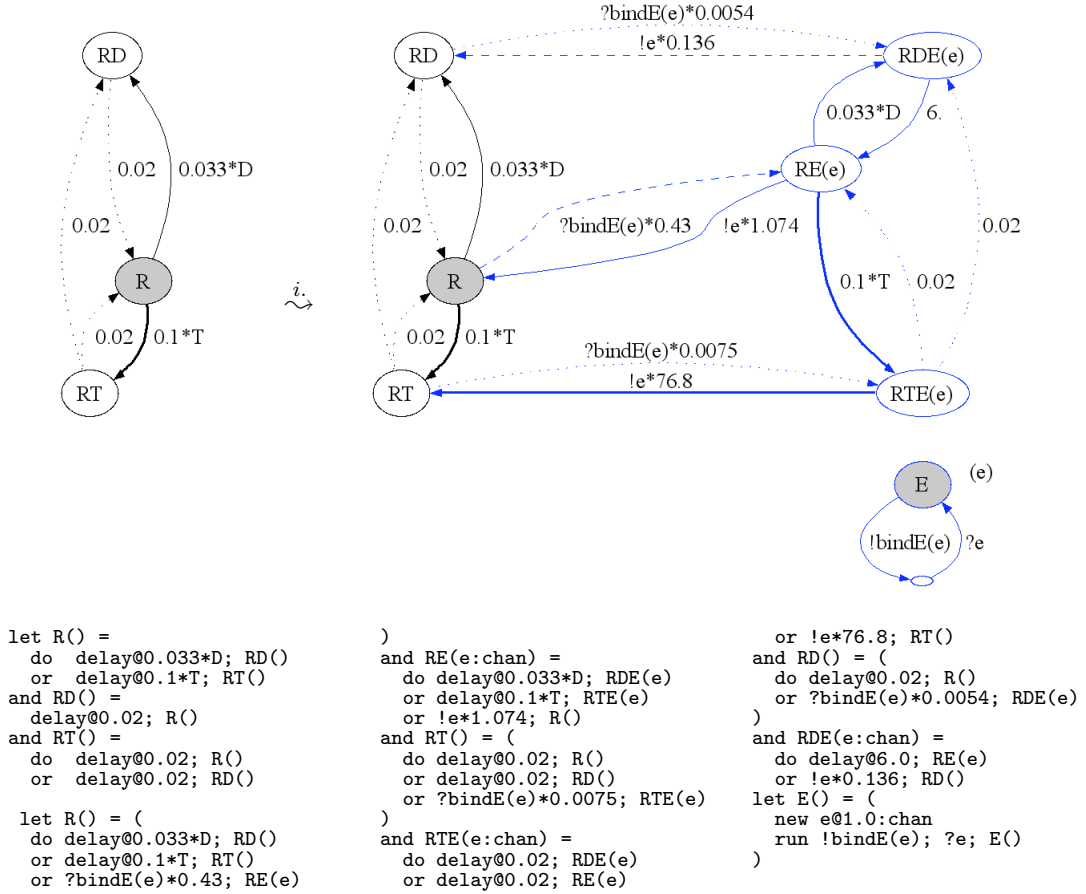


Fig. 7. Compositional construction of the process model for the Rho GTP-binding proteins with GEF and without GAP with respect to  $\overset{i}{\sim}$  in Figure 4.

$E_0$  range between  $10^{-2}\mu M$  and  $10^6\mu M$ . In these simulations, the rate values are given with the unit  $\mu M^{-1}$ . Because of this, we encode  $1\mu M$  of a species as 1 instance of the process in the model at the start of the simulation. For instance, when we start the simulation with  $E_0 = 1000$ , this corresponds to  $1000\mu M$  in the ODE model. In order to be able to run simulations when the initial concentration of species is too low for meaningful stochastic simulations or too high from the point of view of computational resources, we do a scaling by means of scaling factor. This scaling can be seen to be performed on the underlying chemical reactions, that is, we divide the rates of the underlying binary chemical reactions and multiply the initial concentrations of the species with a factoring constant [28]. For instance, in order to run a simulation for the case where there are  $10^{-2}\mu M$  of R and  $10^{-2}\mu M$  of E, we scale the rate values by a factor of  $10^4$ , which allows to give the initial values as  $10^{-2} * 10^4 = 10^2$ . For this purpose, we divide the rates of the interaction channels in the process model with our scaling factor, e.g.,  $10^4$ .

The outcome of our SPiM simulations, reflecting the RT/R<sub>0</sub> ratio at the stable state, are depicted as the graph on the right-hand-side of Figure 8. In Figure 8, the graph on the left-hand-side is the outcome of the ODE simulations taken from [13]. In both graphs, the values are given in logarithms of the concentrations in the

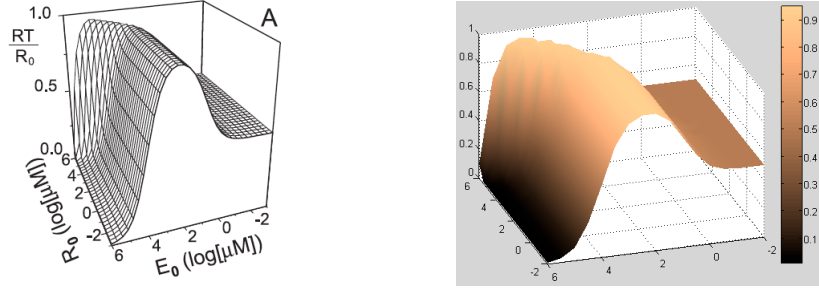


Fig. 8. Graphs displaying the  $RT/R_0$  ratio as the output of the ODE [13] and process simulations, respectively, for the models for Rho GTP-binding proteins with GEF and without GAP.

ODE model and the amount of present processes in the process model, at the start of the respective simulations. For instance, the point in the plot where  $E_0 = 4$  and  $R_0 = 2$  is the case where the simulation is started with  $10^4 = 10000$  E processes and  $10^2 = 100$  R processes. We observe that the outcome of our simulations is consistent with the outcome of the ODE simulations. In order to obtain this match between these different models, the quantitative data consisting of the initial concentrations and rate values of the reactions had to be carefully analysed. This turned out to be a challenging task which required a non-trivial interpretation of the data given in [13] in terms of processes.

### 3.4 Rho GTP-binding Proteins with GEF and GAP

We extend the model in Subsection 3.3 as in Figure 4 (*ii.*), and obtain process model for Rho GTP-binding proteins with GEF and GAP. The graphical representation of this model is depicted in Figure 9 with three interacting processes: one for the Rho GTP-binding protein, which extends the model given in the previous subsection, one for GEF (E) and one for GAP (A).

When we run a simulation using this code with 1000 R, 10 A and 1000 E processes ( $R_0 = 1000$ ,  $A_0 = 10$  and  $E_0 = 1000$ ), we get the right-most plot in Figure 5. We can then read from this plot that the recovery time is approximately 0.5 mins. At the stable state, the  $RT/R_0$  ratio is 0.35.

In order to compare this model with the model in [13], we ran simulations on a range of initial number of molecules, where  $R_0$  is 1000 and  $E_0$  ranges between  $10^{-1}\mu M$  and  $10^4\mu M$ , and  $A_0$  ranges between  $10^{-2}\mu M$  and  $10^2\mu M$ . For some simulations, we performed a scaling as described for the simulations in Subsection 3.3.

The outcome of our simulations are depicted as the graph on the right-hand-side of Figure 10, where the graph on the left-hand-side is the outcome of the ODE simulations taken from [13]. In both graphs, the values are given in logarithms of the concentrations in the ODE model and the amount of present species in the process model, at the beginning of the respective simulations. Again, the outcome of these simulations is consistent with the outcome of the ODE simulations.

Fig.7  $\rightsquigarrow$

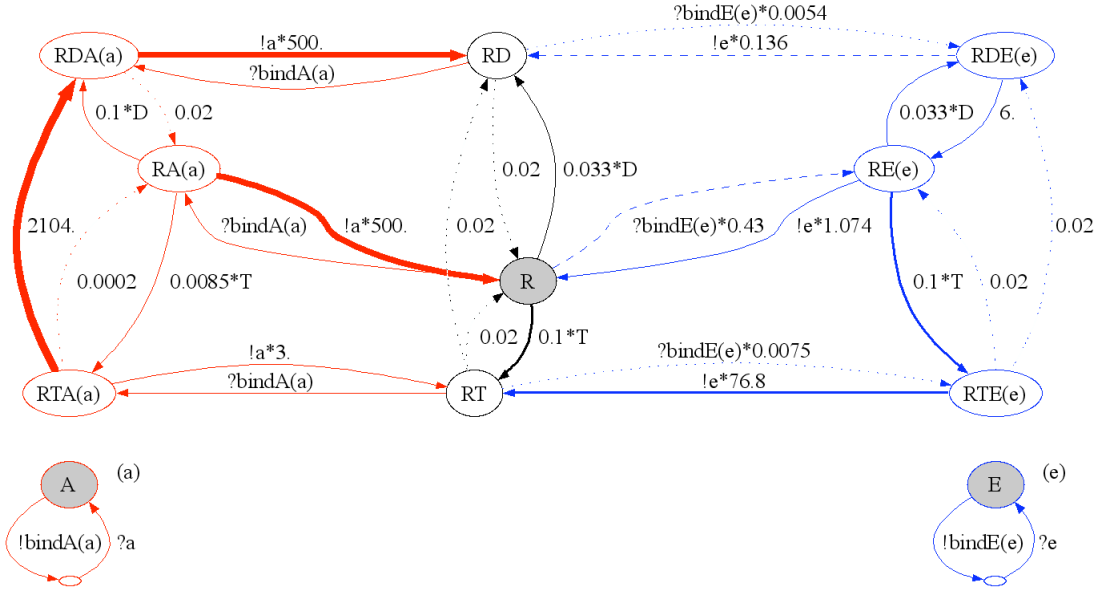


Fig. 9. Compositional construction of the process model for the Rho GTP-binding proteins with GEF and GAP with respect to  $\rightsquigarrow$  in Figure 4.

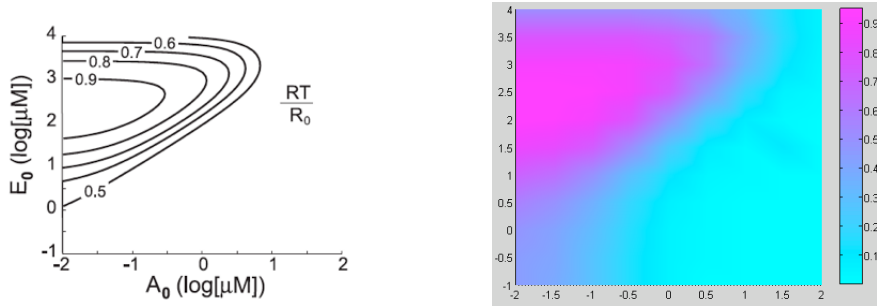


Fig. 10. Graphs displaying the  $RT/R_0$  ratio as the output of the ODE [13] and process simulations, respectively, for the models for Rho GTP-binding proteins with GEF and GAP.

## 4 Extending the Model with Effectors and GDI

Besides the regulators GEF and GAP, the Rho GTP cycle depicted in Figure 1 is affected by interactions with another regulator called GDI and also by interactions with effectors: some effectors for Rho GTP-binding proteins, such as WASP, change their structural conformation and gain the ability to bind to other proteins while they are associated with the active GTP-bound Rho protein attached to the membrane. In the following, based on the model in [13], we first extend our model in a way which takes interactions with effectors into consideration. Following this, we extend our model with GDIs (Guanine-nucleotide Dissociation Inhibitors) which form a class of regulatory proteins for the Rho GTP cycle [7,8,9].

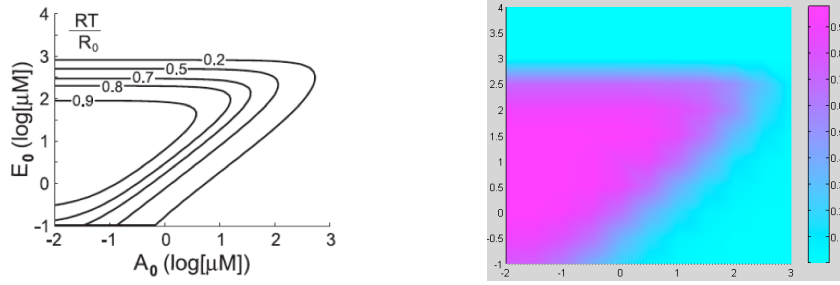


Fig. 11. Graphs displaying the  $RT/R_0$  ratio as the output of the ODE [13] and process simulations, respectively, for the models for Rho GTP-binding proteins with GEF, GAP and effectors.

#### 4.1 Extending the Model with Effectors

The biological function of the GTP-binding proteins is performed only by the active GTP-bound form that binds and activates a broad range of effector proteins. By disregarding the role played by the GDIs, [13] gives a model that extends the model in Subsection 3.4 with effectors. The model is obtained by extending the model of GTP-binding protein cycle with reactions that capture the behaviour of these proteins together with the effectors: an effector protein complex forms a stable complex with GEF (E) at all times. The binding of E to the RT results in the formation of an activated tripartite complex, consisting of RT, E and the effector protein. In this model, M denotes this complex. Due to the lack of detailed data in the literature, the authors suggest that such a representation provides a sufficiently abstract model of the actual biological system. The resulting simplified model extends the model depicted in Figure 2 with the reactions



where the rates of the reactions  $r_1$ ,  $r_2$ , and  $r_3$  are estimated and set as  $600 \mu M^{-1} \cdot \text{min}^{-1}$ ,  $18 \text{ min}^{-1}$  and  $0.6 \mu M^{-1} \cdot \text{min}^{-1}$ , respectively. The authors argue that this model abstracts away from the actual biological kinetics that would involve 54 more reaction rate constants because of the nine intermediate species formed by different complexes of E with RD, RT or E together with an effector.

Using the reactions and rates given above, we extend the process model of Subsection 3.4. For a comparison with the model of [13], we ran simulations on a range of initial number of molecules, where  $R_0$  is 1000,  $E_0$  ranges between  $10^{-1} \mu M$  and  $10^4 \mu M$ , and  $A_0$  ranges between  $10^{-2} \mu M$  and  $10^3 \mu M$ .

The outcome of our simulations are depicted as the graph on the right-hand-side of Figure 11, where the graph on the left-hand-side is the outcome of the ODE simulations taken from [13]. In both graphs, the values are given in logarithms of the concentrations in the ODE model and the amount of represented species in the process model, at the beginning of the respective simulations. Again, the outcome of these simulations is consistent with the outcome of the ODE simulations.

#### 4.2 Extending the Model with GDIs

GDIs were initially identified as down-regulators of GTP-binding proteins due to their ability to prevent the dissociation of GDP from the GTP-binding proteins [7]. This view of GDIs rules out their binding capability with the active GTP-bound

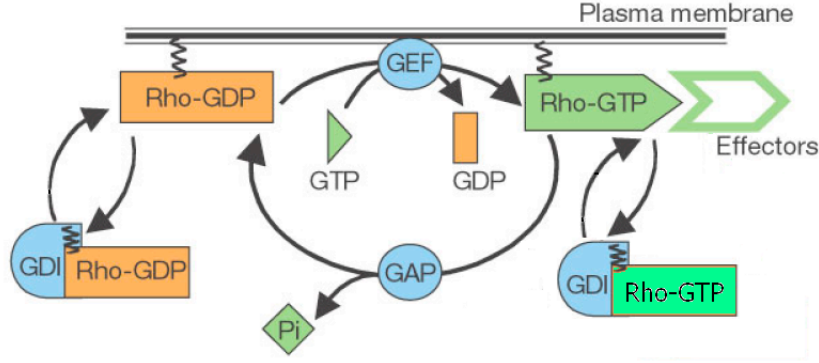
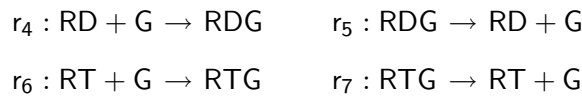


Fig. 12. Rho GTP-binding protein cycle, where GDIs also bind to Rho-GTP. Adapted with permission from Macmillan Publishers Ltd: *Nature* [10], copyright 2002.

form of Rho GTP-binding proteins [16,14]. However, recent evidence (see, e.g., [23,7]) suggests that GDI do not only associate to Rho-GDP, but also to Rho-GTP (see Figure 12 in contrast to Figure 1), and the ability to bind to both Rho-GDP and Rho-GTP contributes to a crucial regulatory mechanism with which GDIs serve as transport proteins, shuttling Rho family proteins between cytosol and membrane in their active and inactive form (see, e.g., [7,8,9]). It is now believed that the complementary structures of GTP-binding proteins and GDIs is crucial in this transport mechanism. When associated to the membrane, GTP-binding proteins are anchored to the membrane by lipid modification on their C-terminus. However, when GTP-binding proteins interact with GDIs, they establish a bond such that the C-terminal domain of GDI binds both the C-terminus and the switch 2 region of the GTP-binding protein, while the N-terminal domain of the GDI binds the switch 1 and switch 2 regions of the GTP-binding protein. This interaction results in a blocking mechanism that prevents the anchoring of the GTP-binding protein to the membrane, and thus the dissociation of GDP or GTP [7]. Thereby GDI prevents both the activation of Rho proteins and their interaction with downstream effectors.

Along these lines, there are various models of the exact role of the GDI. We adopt a model which is hybrid between the two models given in Figure 13 [8]. We describe this model with the following reactions:



During the interaction of the GTP-bound Rho protein with an effector, GTP hydrolysis facilitated by a GAP protein terminates the signal by inducing the GTP hydrolysis. As a consequence Rho no longer interacts with the effector. This allows GDI to bind GDP-bound Rho and extract Rho from the membrane (reaction  $r_4$ , 5 in Figure 13). A complex formed by GDP-bound Rho and GDI is then in the cytosol; a displacement factor or signal at the membrane localises the complex proximal to a membrane compartment (reaction  $r_5$ , 1 in Figure 13). GDI might also extract the Rho protein from the membrane in its GTP-bound form to either terminate the signal prematurely (reaction  $r_6$ , 6 in Figure 13) or to redirect the Rho protein to a distinct membrane within the cell (reaction  $r_7$ , 9 in Figure 13) [23].

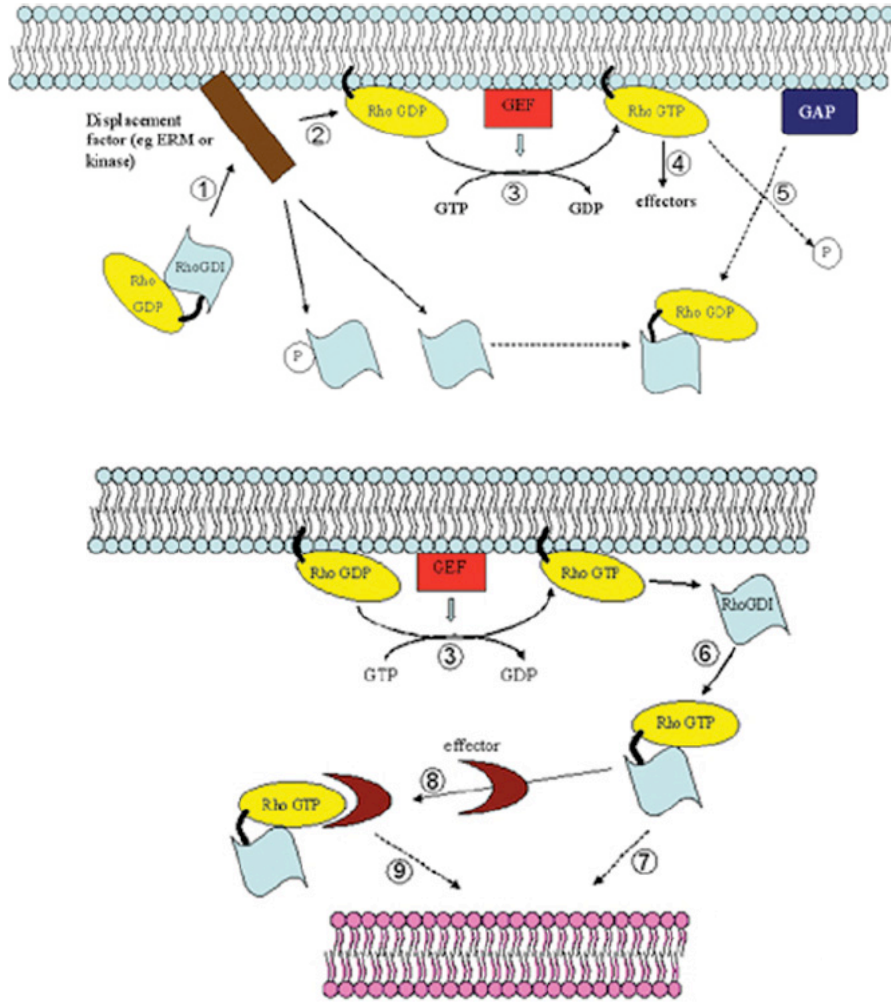


Fig. 13. Two different models, given in [8], for the regulation of Rho family GTP-binding proteins by RhoGDI molecules. We give a model hybrid between these two models.

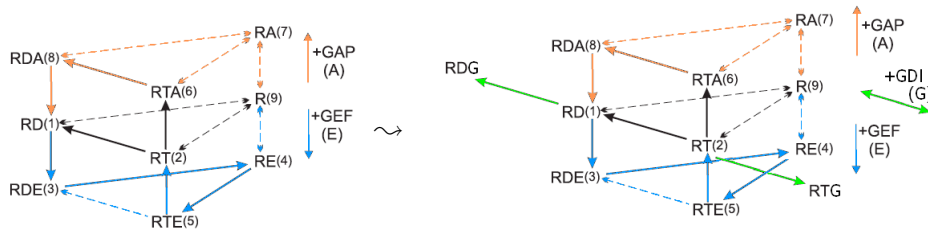


Fig. 14. A graphical representation of the extension of the model depicted in Figure 4 with GDI (G).

The reactions  $r_4$ ,  $r_5$ ,  $r_6$  and  $r_7$  above provide an abstraction of the interactions of GDIs with the GTP-binding protein cycle in the actual biological system. It is possible to work with more complicated models: for example, those involving reactions for the association of different combinations of R, RD and RT with A and E together with G. Because of the evidence with respect to the protein structure of the GDIs which suggests that these reactions have very low affinity [26], we work with a model which abstracts away from such reactions.

We extend our model as depicted in Figure 14 to include the reactions for the GDI and obtain a process model with the graphical representation depicted in Figure 15. In this model, there are four interacting processes: one for the Rho GTP-binding protein, one for GEF, one for GAP and one for GDI. The SPiM code of this model is given in the Appendix and the ODEs for this model are given in Figure A.1.

In [8,18], it is reported that RhoGDIs can bind to different members of the Rho GTPase family, also depending on being in vitro or in vivo. For instance, RhoGDI $\alpha$  can bind to RhoA, RhoB, Rac1, Rac2 and Cdc42 both in vitro and in vivo, whereas RhoGDI $\beta$  may bind several of these GTPases in vitro although not all of these complexes have been detected in vivo. In [9,7], it is also reported that GDIs are outnumbered by GEF and GAP regulators. Furthermore, the molar amount of GDI is in excess of any particular Rho protein, but roughly equal to the total levels of the RhoA, Rac1 and Cdc42 Rho proteins in these cells. In human neutrophils, RhoA, Rac1/Rac2 and Cdc42 are also equimolar with overall GDI levels, and exist largely as cytosolic GDI complexes.

By resorting to this data on the quantity of GDI molecules in the cell, we ran simulations on our model in order to see the effect of varying number of GDIs on the Rho GTP cycle while remaining in the high activity regime of initial concentrations for the R, E and A molecules. This corresponds to transition regime from blue

Fig. 7  $\rightsquigarrow$  *ii.*

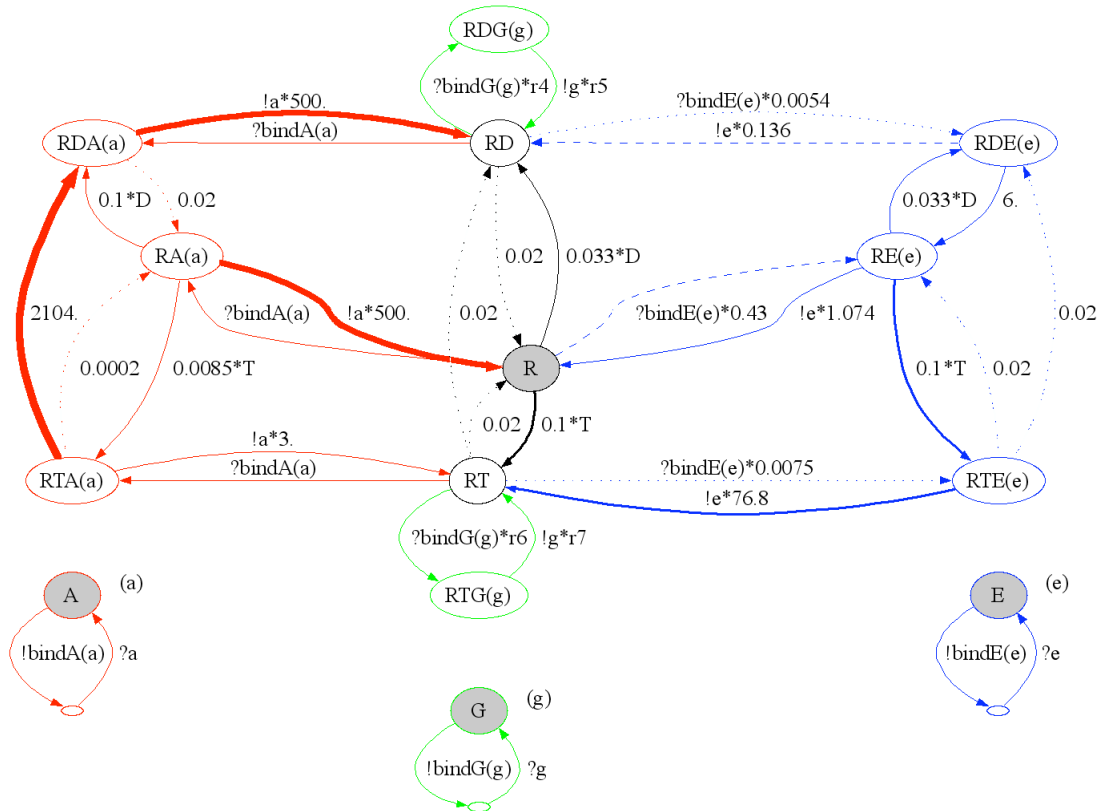


Fig. 15. The graphical representation of the model with GDIs, extending the model depicted in Figure 9.

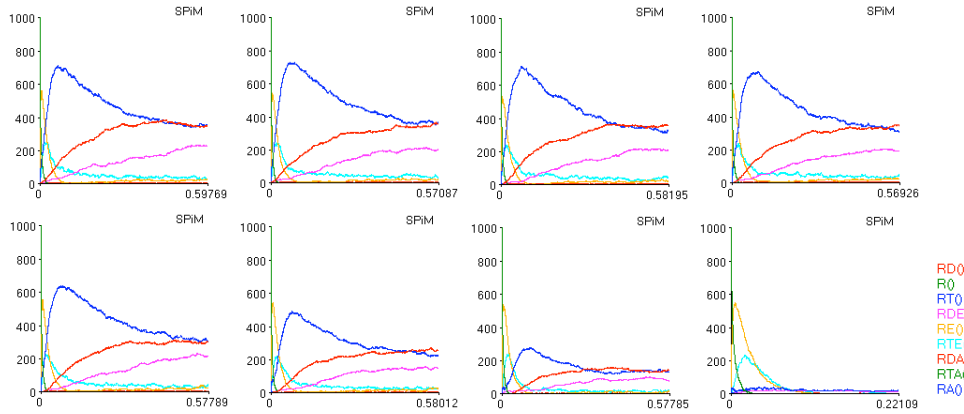


Fig. 16. SPiM plots of simulations with the model which extends GTP-binding protein cycle with GDI and effectors. The  $x$ -axis is the time in minutes and  $y$ -axis is the number of processes. The legend on the right is for all the the plots. In all the simulations,  $R_0$  and  $E_0$  are 1000;  $A_0$  is 10. From left to right, the  $G_0$  value is 0, 10, 30, 60, 100, 300, 600 and 1000.

to red on the plot given on the right-hand-side in Figure 10. For instance, when we consider the initial number of processes as  $R_0$  and  $E_0$  are 1000, and  $A_0$  is 10, we observe that the  $RT/R_0$  ratio at the steady state is 0.35. The outcome of 8 simulations, where  $R_0 = 1000$ ,  $E_0 = 1000$ ,  $A_0 = 10$  and  $G_0$  is varied for the values 0, 10, 30, 60, 100, 300, 600 and 1000, are shown in Figure 16. There, the rate parameters for the reactions  $r_4$ ,  $r_5$ ,  $r_6$  and  $r_7$  are set to 1.0.

As demonstrated by these simulations, our model remains consistent with the two roles that GDIs are thought to play: (*i.*) GDI molecules keep the Rho proteins in the cytosol, preventing their interaction with other binding partners. (*ii.*) GDI shuttle Rho proteins between the membrane and the cytosol. These two roles are captured by our model because in the simulations we observe that when G are bound to RT or RD, these processes are not available for any further interaction with any other species of the model, as they would be in the cytosol in the cell. In order to interact with the effectors on the membrane they need to be shuttled back to membrane by G which is modelled by unbinding of RDG and RTG complexes. As a consequence of these two roles, the emergent inhibitory role is also being observed as the decreasing activity when we run simulations with more G processes as demonstrated in Figure 16.

#### 4.3 Parameter Exploration for the GDI reactions

As stated in Section 2, GTP-binding proteins interact with GDIs by establishing a bond such that the C-terminal domain of GDI binds both the C-terminus and the switch 2 region of the GTP-binding protein, while the N-terminal domain of the GDI binds the switch 1 and switch 2 regions of the GTP-binding protein. This interaction results in a blocking mechanism that prevents the anchoring of the GTP-binding protein to the membrane. In [22], it is reported that deleting certain numbers of amino acids from the C-terminal of GDIs affect their binding affinity. Because of this, the authors argue that it is tempting to anticipate proteins related to GDI to demonstrate distinct functional specificities due to differences in the C-terminal. Along these lines, RhoGDI $\alpha$  and RhoGDI $\beta$  have been observed to have different binding affinities for different Rho proteins in vivo and in vitro experiments [8].

Furthermore, in [8], it is also reported that phosphorylation of both the GDIs and the Rho GTP-binding proteins plays a regulatory role on the affinity of the interactions between Rho proteins and GDIs.

In this subsection, in order to see the effect of different rate constants modelling different affinities of GDIs, we vary the rate parameters of the reactions  $r_4$ ,  $r_5$ ,  $r_6$  and  $r_7$  in our model between  $10^{-4}$  and  $10^4$ . For this purpose, we first ran simulations with 600 G (GDI) processes. In these simulations, we set the parameters of the reactions  $r_4$  and  $r_5$  to one of  $10^{-4}$ ,  $10^0$  and  $10^4$  which results in 9 cases. We then observe the behaviour of the  $RT/R_0$  ratio when the rates of the reactions  $r_6$  and  $r_7$  are varied between  $10^{-4}$  and  $10^4$  with an order of magnitude of 1. We get the graphs in Figure 17, displaying the  $RT/R_0$  ratio with varying rate parameters at these  $9 \times 9 \times 9$  number of simulations. We then ran simulations with 300 G processes, however from the symmetric point of view: we set the parameters of the reactions  $r_6$  and  $r_7$  to one of  $10^{-4}$ ,  $10^0$  and  $10^4$  which results in 9 cases, where the rates of the reactions  $r_4$  and  $r_5$  are varied between  $10^{-4}$  and  $10^4$  with an order of magnitude of 1. For these simulations, we get the graphs in Figure 18, displaying the  $RT/R_0$  at these  $9 \times 9 \times 9$  number of simulations.

In the first set of simulations, at the steady state we observe a plateau at 0.1 for the cases where  $r_4 \geq r_5$  with the exception of the case where  $r_4 = 10^{-4}$ ,  $r_5 = 10^{-4}$ , as depicted in Figure 17. A mechanistic explanation of these simulations is as follows: the value of  $RT/R_0$  remains constant at approximately 0.1, which corresponds to

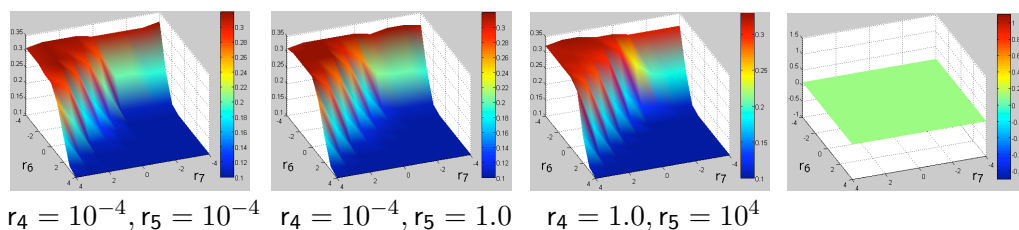


Fig. 17. The result of the simulations with respect to  $RT/R_0$  ratio at the  $z$ -axis, where  $R_0$  and  $E_0$  are set to 1000.  $A_0$  is 10 and  $G_0$  is 600. The  $x$  and  $y$ -axis are the parameters for the reactions  $r_6$  and  $r_7$  varying between  $10^{-4}$  and  $10^4$ . For the case where  $r_4 = 10^{-4}$  and  $r_5 = 10^4$ , we observe a plot similar to those on the left above. We observe a plateau at 0.1, as in the right-most plot, for the cases where  $r_4 = 1.0$ ,  $r_5 = 1.0$ ;  $r_4 = 10^4$ ,  $r_5 = 10^4$ ;  $r_4 = 10^4$ ,  $r_5 = 1.0$ ;  $r_4 = 10^4$ ,  $r_5 = 10^{-4}$  and  $r_4 = 1.0$ ,  $r_5 = 10^{-4}$ .

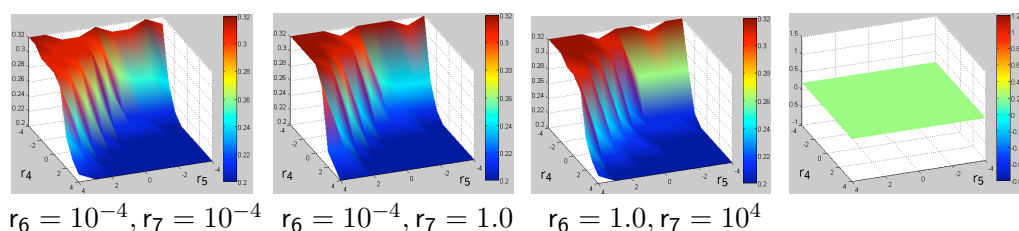


Fig. 18. The result of the simulations with respect to  $RT/R_0$  ratio at the  $z$ -axis, where  $R_0$  and  $E_0$  are set to 1000.  $A_0$  is 10 and  $G_0$  is 300. The  $x$  and  $y$ -axis are the parameters for the reactions  $r_4$  and  $r_5$  varying between  $10^{-4}$  and  $10^4$ . For the case where  $r_6 = 10^{-4}$  and  $r_7 = 10^4$ , we observe a plot similar to those on the left above. We observe a plateau at 0.2, as in the right-most plot, for the cases where  $r_6 = 1.0$ ,  $r_7 = 10^{-4}$ ;  $r_6 = 1.0$ ,  $r_7 = 1.0$ ;  $r_6 = 10^4$ ,  $r_7 = 10^{-4}$ ;  $r_6 = 10^4$ ,  $r_7 = 1.0$  and  $r_6 = 10^4$ ,  $r_7 = 10^4$ .

a steady state of 100 RT. In fact, if we set  $R_0 = 400$  and  $G_0 = 0$  we also obtain the same steady state, suggesting that all of the GDI (G) proteins are bound in the plateau region. Indeed, on closer examination of the individual simulations we do observe that almost all GDI proteins are bound to Rho, either in the RD or RT form. Since there are 600 GDI proteins in the system, this means that only 400 Rho proteins remain, resulting in a steady state of about 100 RT, with the rest of the Rho proteins in different states.

The cases where  $r_4 \geq r_5$  are those where the binding rate  $r_4$  is sufficiently high to shift the steady state such that all the available G processes get bound. For instance, if  $r_4 = r_5 = 1$ , the equilibrium of the RD - RDG reaction is shifted in favour of RDG (due to the larger numbers of RD molecules), and (almost all of) the GDIs end up in a bound state, regardless of the values of  $r_6$  and  $r_7$ . If the latter two rates are low, then most of the GDI bind to RD. However, for the cases where  $r_4 = r_5 = 10^{-4}$  and  $r_4 < r_5$ , we do not observe this plateau because  $r_4$  is too low in comparison to the rates of the rest of the system in order to bind all the G processes. Then, reaching the steady state at 0.1 requires the regulation of the system by  $r_6$  and  $r_7$ . In that case, the steady state at 0.1 is reached when  $r_6$  is sufficiently high with respect to  $r_7$ .

The second set of simulations reflect the same situation from a symmetric point of view, as depicted in Figure 18. In these simulations, we observe a plateau for the cases where  $r_6 \geq r_7$  with the exception of the case where  $r_6 = 10^{-4}$ ,  $r_7 = 10^{-4}$ . However, in these latter simulations, the plateau is at 0.2 in contrast to the plateau at 0.1 in the first set of simulations. This is because of the 300 G processes at the beginning of the simulations in contrast to 600 G processes in the first set of simulations. From this symmetric point of view, the cases where  $r_6 \geq r_7$  are those where the binding rate of  $r_6$  is sufficiently high to shift the steady state such that all the available G get bound. As the the rate of  $r_6$  increases relative to  $r_7$  and  $r_4$ , more of the GDI become bound to RT, but without affecting the overall levels of free RT in the system. Similar to the case in the first set of simulations where  $r_4 = 10^{-4}$ , in the case where  $r_6 = 10^{-4}$ , in order to obtain the steady state level of RT at 0.2, the system needs to be regulated by  $r_4$  and  $r_5$  such that  $r_4$  is sufficiently high with respect to  $r_5$ .

The rates  $r_4$ ,  $r_5$ ,  $r_6$  and  $r_7$  together determine the effectiveness of GDI in removing Rho from the system, and therefore in decreasing the overall activity of RT. However, determined by the relative rate of  $r_4$  and  $r_5$  in comparison to that of  $r_6$  and  $r_7$ , and vice versa, Rho can be removed from the system (that is, shuttled from

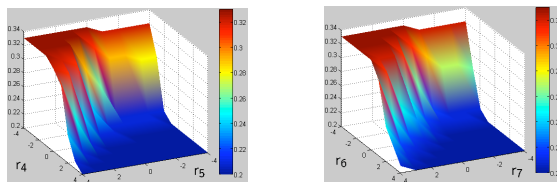


Fig. 19. The result of the simulations with respect to RT/ $R_0$  ratio at the  $z$ -axis, where  $R_0$  and  $E_0$  are set to 1000.  $A_0$  is 10 and  $G_0$  is 300. In the simulations on the left-hand-side, the reactions  $r_6$  and  $r_7$  are removed from the system, and on the right-hand-side, the reactions  $r_4$  and  $r_5$  are removed. The  $x$  and  $y$ -axis are the parameters for the reactions  $r_4$  and  $r_5$  on the left, and for the reactions  $r_6$  and  $r_7$  on the right, varying between  $10^{-4}$  and  $10^4$ .

the membrane to the cytosol) as RT or RD. Indeed, when both  $r_4$  and  $r_6$  are sufficiently low, we do not observe a decrease in the RT/R<sub>0</sub> ratio. This observation supports the view on the regulation of the affinity of Rho and GDI interactions by phosphorylation of these proteins. This is because different phosphorylation conditions may result in different affinities of GDI to Rho-GTP and Rho-GDP. In order to test this view, we performed simulations where we removed the reactions  $r_4$  and  $r_5$  or we removed the reactions  $r_6$  and  $r_7$  by setting their rates to 0. As a result of these simulations, depicted in Figure 19, for the case where  $r_6 = r_7 = 0$ , we observe a behaviour similar to those in Figure 18 where  $r_6$  is sufficiently low. Similarly, for the case where  $r_4 = r_5 = 0$ , we observe a behaviour similar to those in Figure 17 where  $r_4$  is sufficiently low. These observations support the view that binding of GDI to RT and RD to extract these proteins from the membrane is sensitive to regulation of their interaction affinities.

To conclude, our model captures the behaviour of the GDI at the membrane binding to Rho proteins to perform their inhibitory role by extracting Rho proteins from the Rho GDP-GTP cycle, and the simultaneous shuttling behaviour of Rho by GDI. This is because extracted Rho can be considered to be in the cytosol and delivered to remote membranes inside the cell. Our results indicate that in our model as long as the association rates are sufficiently high with respect to the disassociation rates, the inhibitory role of GDI is not hampered. However, by varying the relative rates of Rho-GDP, GDI association and Rho-GTP, GDI association, it is possible to observe a modification in the relative concentrations of RDG and RTG.

## 5 A Modular View of Interactions

The Rho family of GTP-binding proteins have 22 human members. In cellular events such as phagocytosis, some of these proteins act together regulating different parts of the event. In fact, in biological systems, there are often classes of biochemical species which share the same structure in their interactions with their partners. For example, the Rho GTP-binding proteins Rac and Cdc42 act in parallel as molecular switches at different stages of Fc receptor-mediated phagocytosis (see Section 2). The interactions of these GTP-binding proteins with their effectors are regulated by classes of GEF, GAP and GDI, however with possibly different rates.

It is desirable to represent the interactions of such classes of species with their partner classes of species in a single modular model, which can be instantiated by its parameters to simulate different members of a class of species. For instance, consider the hypothetical model depicted in Figure 20: in this model, a class  $A$  of species has  $n$  members that have different interaction affinities with another class  $B$  of species. Here, we can consider  $A$  to be different members of the Rho GTP-binding proteins and  $B$  as a collection of different GEF and GAP proteins with varying affinities to different Rho. In the following, we introduce a technique to represent such a model modularly, such that each member of a class of species can be given as an instance of a process expression that we call *affinity map*.

**Definition 5.1** Let  $\mathcal{A} = \{A_1, \dots, A_n\}$  and  $\mathcal{B} = \{B_1, \dots, B_m\}$  be two classes of species such that each  $A_i \in \mathcal{A}$  can be bound to at most one  $B_j \in \mathcal{B}$  at any given

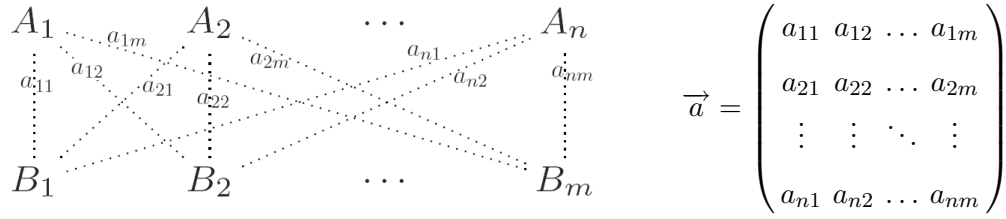


Fig. 20. A graphical representation of two classes of species that can interact with each other and the matrix representation of their interaction channels.

time. Each  $A_i$  and  $B_j$  can bind by interacting on the channel  $a_{ij}$ , as depicted in Figure 20, with a rate  $r_{ij} \geq 0$  and they can unbind with a rate  $t_{ij} \geq 0$ . Let  $\vec{a}$  be the matrix depicted in Figure 20 and let each  $x_{ij}$  be a variable for each  $a_{ij}$ . The *affinity map* of  $\mathcal{A}$  and  $\mathcal{B}$  is defined as follows, where we use  $\vec{x}$  as an abbreviation for the expression  $x_{11}:\text{chan}(\text{chan}), \dots, x_{nm}:\text{chan}(\text{chan})$ , and  $\mathbf{a0}$  and  $\mathbf{e0}$  are channels with rate 0.0.

```

new e0@0.0:chan()
let A( $\vec{x}$ ) = (
  new e11@t11:chan() new e12@t12:chan() ... new e1m@t1m:chan()
  new e21@t21:chan() new e22@t22:chan() ... new e2m@t2m:chan()
  ...
  new en1@tn1:chan() new en2@tn2:chan() ... new enm@tnm:chan()
do !x11(e11); Ab(e11,  $\underbrace{\mathbf{e0}, \dots, \mathbf{e0}}_{(n-1) \times}$ ) or ... or !x1m(e1m); Ab(e1m,  $\underbrace{\mathbf{e0}, \dots, \mathbf{e0}}_{(n-1) \times}$ )
or !x21(e21); Ab( $\mathbf{e0}, e_{21}, \dots, \mathbf{e0}$ ) or ... or !x1m(e2m); Ab( $\mathbf{e0}, e_{2m}, \dots, \mathbf{e0}$ )
...
or !xn1(en1); Ab( $\underbrace{\mathbf{e0}, \dots, \mathbf{e0}}_{(n-1) \times}, e_{n1}$ ) or ... or !xnm(enm); Ab( $\underbrace{\mathbf{e0}, \dots, \mathbf{e0}}_{(n-1) \times}, e_{nm}$ )
and Ab(e1:chan, ..., en:chan) = do !e1; A( $\vec{x}$ ) or ... or !en; A( $\vec{x}$ )

```

```

let B( $\vec{x}$ ) =
  do ?x11(e); Bb(e,  $\underbrace{\mathbf{e0}, \dots, \mathbf{e0}}_{(m-1) \times}$ ) or ... or ?xn1(e); Bb(e,  $\underbrace{\mathbf{e0}, \dots, \mathbf{e0}}_{(m-1) \times}$ )
  or ?x12(e); Bb( $\mathbf{e0}, e, \dots, \mathbf{e0}$ ) or ... or ?xn2(e); Bb( $\mathbf{e0}, e, \dots, \mathbf{e0}$ )
  ...
  or ?x1m(e); Bb( $\underbrace{\mathbf{e0}, \dots, \mathbf{e0}}_{(m-1) \times}, e$ ) or ... or ?xnm(e); Bb( $\underbrace{\mathbf{e0}, \dots, \mathbf{e0}}_{(m-1) \times}, e$ )

```

and  $\text{Bb}(e_1:\text{chan}, \dots, e_m:\text{chan}) = \text{do } ?e_1; B(\vec{x}) \text{ or } \dots \text{ or } ?e_m; B(\vec{x})$

```

new a11@r11:chan(chan) ... new a1m@r1m:chan(chan)
new a21@r21:chan(chan) ... new a2m@r2m:chan(chan)
...
new an1@rn1:chan(chan) ... new anm@rnm:chan(chan)
new a0@0.0:chan(chan)

```

Affinity maps provide a modular view of classes of interacting species. By instantiating affinity maps, we can provide more refined models for different members of a class of species, and in a simulation use only specific binding capabilities of these members. For this purpose, we introduce the notion of *projection*, which serves to isolate members of a class of species and their binding capabilities, relevant to the simulation being considered.

**Definition 5.2** The *i*-row-projection of a matrix  $\vec{a}$ , denoted by  $\vec{a}_i$ , is the matrix obtained from  $\vec{a}$  by replacing all the elements that are not in the *i*-th row with  $\mathbf{a0}$ . The *j*-column-projection of a matrix  $\vec{a}$ , denoted by  $\vec{a}^j$ , is the matrix obtained from  $\vec{a}$  by replacing all the elements that are not in the *j*-th column with  $\mathbf{a0}$ .

**Proposition 5.3** Let  $A(\vec{x})$  and  $B(\vec{x})$  be defined as in the affinity map of  $\mathcal{A} = \{A_1, \dots, A_n\}$  and  $\mathcal{B} = \{B_1, \dots, B_m\}$  in Definition 5.1. Then  $A(\vec{a}_i)$  and  $B(\vec{a}^j)$  are equivalent to the following expressions with respect to the semantics of stochastic  $\pi$ -calculus, implemented in SPiM.

$$A(\vec{a}_i) = ( \text{new } e_{i1}@t_{i1}:\text{chan}() \text{ new } e_{i2}@t_{i2}:\text{chan}() \dots \text{ new } e_{im}@t_{im}:\text{chan}() \\ \text{do } !a_{i1}(e_{i1}); !e_{i1}; A(\vec{a}_i) \text{ or } \dots \text{ or } !a_{im}(e_{im}); !e_{im}; A(\vec{a}_i) )$$

$$B(\vec{a}^j) = \text{do } ?a_{1j}(e); ?e; B(\vec{a}^j) \text{ or } \dots \text{ or } ?a_{nj}(e); ?e; B(\vec{a}^j)$$

**Proof.** Proof by induction on *n* and *m*: the rate of the channel  $\mathbf{a0}$  is 0.0. When the channels in the affinity map are instantiated with this channel, processes that interact by these channels do not have an effect on the stochastic behaviour of the system, because they are equivalent to zero process  $()$ . Thus, expressions with this channel and their continuations can be removed. This results in the expressions given above.  $\square$

By using this idea, we can describe, for instance, species  $A_1$  in Figure 20 as  $A(\vec{a}_1)$ , and species  $B_2$  as  $B(\vec{a}^2)$ .

## 6 Discussion

We have given a process model of the Rho GTP-binding protein cycle, and run simulations of our model using the SPiM tool [21]. Our model closely follows Goryachev and Pokhilko's paper [13], which provides an ODE analysis of the Rho GTP-binding

protein cycle, both in isolation and with effectors. The use of process algebra techniques to model and simulate biological systems, and the comparison with the ODE analysis is not new, see for example [17,4]. Our results do however provide an essential calibration between our process-algebra techniques and the ODE analysis for the basic model of the Rho GTP-binding protein cycle. Moreover, the extension that we have introduced to the stochastic  $\pi$ -calculus provides a more modular means for extending and refining the models. With the initial calibration of our model, we now have the freedom to exploit the compositionality of the process-algebra approach to study more refined systems by extending our basic model. Although the ODE approach can also be extended, we believe the extension is less natural and ultimately will not scale to large biological systems.

In this paper, we have extended our basic model to capture the effect of the GDIs in the Rho GTP-binding protein cycle. For this purpose, we use the biological models described in the biological literature in a way which better reflects the current knowledge on GDIs [7,8,9], in contrast to the former view of these proteins [16,14]. In order to obtain a quantitative analysis of the extended model by means of simulations, we have varied the initial number of species and rate parameters, also by taking the biological literature on GDIs into consideration. An analysis of the parameter space with respect to the extended model required extending the SPiM tool with parameter exploration capabilities. Further development of SPiM tool with such parameter exploration capabilities is a topic of ongoing work which is also being directly influenced from the work presented in this paper.

Rho GTP-binding proteins serve as molecular switches in various cellular activities, including phagocytosis. Our long-term goal is to use the model of this paper as a generic model for these proteins which can be compositionally plugged into larger models. By gradually extending the model and moving between levels of abstractions, we hope to eventually deliver models for larger biological systems, such as phagocytosis, where Rho proteins are important components. Along these lines, the technique that we have introduced for modular representation of interacting species should be useful to represent more complex biological systems such as Fc receptor mediated phagocytosis, where different Rho proteins act in concert. Another topic of ongoing investigation is exploiting the biological data available in the literature to obtain more detailed models from the point of view biological hypothesis generation. Our ultimate goal is benefiting from models constructed this way, by iterating between biological feedback and extensive computer simulations, in the development of useful systems biology tools as well as interesting biological hypothesis.

## A Program code for the model with GDIs in Fig. 15.

```
directive sample 40.0 1000          val D = 50.0 val T = 500.0
directive plot
RDA(a); RTA(a); RA(a); RD();       new bindA@1.0:chan(chan)
R(); RT(); RDE(e); RE(e); RTE(e)   new bindE@1.0:chan(chan)
```

$$\begin{aligned}
[RD]^{\bullet} &= k_{81}.RDA - k_{18}.RD.A + k_{31}.RDE - k_{13}.RD.E + k_{91}.R.D - k_{19}.RD + k_{21}.RT + r_5.RDG - r_4.RD.G \\
[RT]^{\bullet} &= k_{52}.RTE - k_{25}.RT.E + k_{92}.R.T - k_{29}.RT - k_{21}.RT + k_{62}.RTA - k_{26}.RT.A + r_7.RTG - r_6.RT.G \\
[RDE]^{\bullet} &= k_{13}.RD.E - k_{31}.RDE + k_{43}.RE.D - k_{34}.RDE + k_{53}.RTE \\
[RE]^{\bullet} &= k_{34}.RDE - k_{43}.RE.D + k_{54}.RTE - k_{45}.RE.T + k_{94}.R.E - k_{49}.RE \\
[RTE]^{\bullet} &= k_{45}.RE.T - k_{54}.RTE + k_{25}.RT.E - k_{52}.RTE - k_{53}.RTE \\
[RTA]^{\bullet} &= k_{26}.RT.A - k_{62}.RTA - k_{68}.RTA + k_{76}.RA.T - k_{67}.RTA \\
[RA]^{\bullet} &= k_{67}.RTA - k_{76}.RA.T + k_{97}.R.A - k_{79}.RA + k_{87}.RDA - k_{78}.RA.D \\
[RDA]^{\bullet} &= k_{68}.RTA + k_{78}.RA.D - k_{87}.RDA + k_{18}.RD.A - k_{81}.RDA \\
[R]^{\bullet} &= k_{29}.RT - k_{92}.R.T + k_{49}.RE - k_{94}.R.E + k_{19}.RD - k_{91}.R.D + k_{79}.RA - k_{97}.R.A \\
[E]^{\bullet} &= k_{31}.RDE - k_{13}.RD.E + k_{52}.RTE - k_{25}.RT.E + k_{49}.RE - k_{94}.R.E \\
[A]^{\bullet} &= k_{81}.RDA - k_{18}.RD.A + k_{62}.RTA - k_{26}.RT.A + k_{79}.RA - k_{97}.R.A \\
[G]^{\bullet} &= r_5.RDG + r_7.RTG - r_4.RD.G - r_6.RT.G \\
[RDG]^{\bullet} &= r_4.RD.G - r_5.RDG \\
[RTG]^{\bullet} &= r_6.RT.G - r_7.RTG
\end{aligned}$$

Fig. A.1. ODEs for the model extended with GDIs. The shaded parts are the those which are added to the ODEs of [13], given in Section 2.3.

```

new bindG@1.0:chan(chan)          do delay@0.02; RDE(e)
                                  or delay@0.02; RE(e)
let R() = (
  do delay@0.033*D; RD()
  or delay@0.1*T; RT()
  or ?bindA(a); RA(a)
  or ?bindE(e)*0.43; RE(e)
)
and RA(a:chan) =
  do delay@0.1*D; RDA(a)
  or delay@0.0085*T; RTA(a)
  or !a*500.0; R()
and RE(e:chan) =
  do delay@0.033*D; RDE(e)
  or delay@0.1*T; RTE(e)
  or !e*1.074; R()
and RT() = (
  do delay@0.02; R()
  or delay@0.02; RD()
  or ?bindA(a); RTA(a)
  or ?bindE(e)*0.0075; RTE(e)
  or ?bindG(g); RTG(g)
)
and RTG(g:chan) = !g; RT()
and RTA(a:chan) =
  do delay@0.0002; RA(a)
  or delay@2104.0; RDA(a)
  or !a*3.0; RT()
and RTE(e:chan) =
  do delay@0.02; RDE(e)
  or !e*500.0; RD()
  and RDA(a:chan) =
    do delay@0.02; RA(a)
    or !a*500.0; RD()
  and RDG(g:chan) = !g; RD()
  and RDE(e:chan) =
    do delay@6.0; RE(e)
    or !e*0.136; RD()
)
let A() = (
  new a@1.0:chan
  run !bindA(a); ?a; A()
)
let E() = (
  new e@1.0:chan
  run !bindE(e); ?e; E()
)
let G() = (
  new g@1.0:chan
  run !bindG(g); ?g; G()
)

```

run 1000 of R()  
run 10 of A()

run 1000 of E()  
run 300 of G()

## References

- [1] Bruce Alberts, Alexander Johnson, Peter Walter, Julian Lewis, Martin Raff, and Keith Roberts. *Molecular Biology of the Cell, Fifth Edition*. Garland Science, 2008.
- [2] Ralf Blossey, Luca Cardelli, and Andrew Phillips. A compositional approach to the stochastic dynamics of gene networks. *Transactions in Computational Systems Biology*, 3939:99–122, 2006.
- [3] Xose R. Bustelo, Vincent Sauzeau, and Inmaculada M. Berenjano. Gtp-binding proteins of the rho/rac family: regulation, effectors and function in vivo. *BioEssays*, 29:356–370, 2007.
- [4] Luca Cardelli. On process rate semantics. *Theoretical Computer Science*, 2007. to appear.
- [5] Luca Cardelli, Emmanuelle Caron, Philippa Gardner, Ozan Kahramanoğ ulları, and Andrew Phillips. A process model of actin polymerisation. In *From Biology To Concurrency and back, satellite Workshop of ICALP'08*, ENTCS. Elsevier, 2008. to appear.
- [6] Giovanni Chimini and Philippe Chavrier. Function of Rho family proteins in actin dynamics during phagocytosis and engulfment. *Nature Cell Biology*, 2:191–196, 2000.
- [7] Céline DerMardirossian and Gary M. Bokoch. GDIs: central regulatory molecules in Rho GTPase activation. *TRENDS in Cell Biology*, 15(7):356–363, 2005.
- [8] Athanasios Dovas and John R. Couchman. RhoGDI: Multiple functions in the regulation of rho family gtpase activities. *Biochemistry Journal*, 390:1–9, 2005.
- [9] Estelle Dransart, Birgitta Olofsson, and Jacqueline Cherfils. RhoGDIs revisited: Novel roles in rho regulation. *Traffic*, 6:957–966, 2005.
- [10] Sandrine Etienne-Manneville and Alan Hall. Rho GTPases in cell biology. *Nature*, 420:629–635, 2002.
- [11] Erick Garcia-Garcia and Carlos Rosales. Signal transduction during fc receptor-mediated phagocytosis. *Journal of Leukocyte Biology*, 72:1092–1108, 2002.
- [12] Daniel T. Gillespie. Exact stochastic simulation of coupled chemical reactions. *The Journal of Physical Chemistry*, 81(25):2340–2361, 1977.
- [13] Andrew B. Goryachev and Alexandra V. Pokhilko. Computational model explains high activity and rapid cycling of rho gtpases within protein complexes. *PLoS Computational Biology*, 2:1511–1521, 2006. For the license terms of the figures adapted from this work, see <http://creativecommons.org/licenses/by/2.5/>.
- [14] Andrew B. Goryachev and Alexandra V. Pokhilko. Dynamics of Cdc42 network embodies a Turing-type mechanism of yeast cell polarity. *FEBS Letters*, 582(10):1437–1443, 2008.
- [15] A.B. Hall, M. A. Gakidis, M Glogauer, J.L. Wilsbacher, S Gao, W. Swat, and J.S. Brugge. Requirements for vav guanine nucleotide exchange factors and rho gtpases in fcγr- and complement-mediated phagocytosis. *Immunity*, 24:305–316, 2006.
- [16] Aron B. Jaffe and Alan Hall. Rho GTPases: Biochemistry and biology. *Annual Review of Cell and Developmental Biology*, 21:247–269, 2005.
- [17] P. Lecca and C. Priami. Cell cycle control in eukaryotes: A BioSpi model. In *Proc. Workshop on Concurrent Models in Molecular Biology (BioConcur'03)*, ENTCS. Elsevier, 2003.
- [18] B. Olofsson. Rho guanine dissociation inhibitors: pivotal molecules in cellular signalling. *Cell Signal.*, 11(8):545–554, 1999.
- [19] J. C. Patel, A. Hall, and E. Caron. Vav regulates activation of rac but not cdc42 during FcγR-mediated phagocytosis. *Molecular Biology of the Cell*, 13:1215–1226, 2002.
- [20] A. Phillips, L. Cardelli, and G. Castagna. A graphical representation for biological processes in the stochastic pi-calculus. *Transactions in Computational Systems Biology*, 4230:123–152, 2006.
- [21] Andrew Phillips and Luca Cardelli. Efficient, correct simulation of biological processes in the stochastic pi-calculus. In *Computational Methods in Systems Biology*, volume 4695 of *LNCS*, pages 184–199. Springer, 2007.
- [22] J. V. Platko, D. A. Leonard, C. N. Adra R. J. Shaw, R. A. Cerione, and B. Lim. A single residue can modify target-binding affinity and activity of the functional domain of the rho-subfamily gdp dissociation inhibitors. *Proc Natl Acad Sci U S A*, 92(7):2974–2978, 1995.

- [23] Miguel Angel Del Pozo, William B. Kiosses, Nazilla B. Alderson, Nahum Meller, Klaus M. Hahn, and Martin Alexander Schwartz. Integrins regulate GTP-Rac localized effector interactions through dissociation of Rho-GDI. *Nature Cell Biology*, 4:232–239, 2002.
- [24] C. Priami, A. Regev, E. Shapiro, and W. Silverman. Application of a stochastic name-passing calculus to representation and simulation of molecular processes. *Information Processing Letters*, 80, 2001.
- [25] C. Priami, A. Regev, E. Shapiro, and W. Silverman. Application of a stochastic name-passing calculus to representation and simulation of molecular processes. *Information Processing Letters*, 80:25–31, 2001.
- [26] Klaus Scheffzek, Ilona Stephan, Ole N. Jensen, Daria Illenberger, and Peter Gierschik. The racrhogdi complex and the structural basis for the regulation of rho proteins by rhogdi. *Nature Structural Biology*, 7:122–126, 2000.
- [27] Joel A. Swanson and Adam D. Hoppe. Cdc42, Rac1, and Rac2 display distinct patterns of activation during phagocytosis. *Molecular Biology of the Cell*, 15(8):3509–3519, 2004.
- [28] O. Wolkenhauer, M. Ullah, W. Kolch, and Cho K.H. Modeling and simulation of intracellular dynamics: choosing an appropriate framework. *IEEE Trans. Nanobioscience*, 3:200–207, 2004.